Available online at www.sciencedirect.com
ScienceDirect
Journal of Magnetic Resonance 182 (2006) 133–142
JMR Journal of Magnetic Resonance
www.elsevier.com/locate/jmr

Combined simulated annealing and Shinnar–Le Roux pulse design of slice-multiplexed RF pulses for multi-slice imaging

K.J. Lee *, M.N.J. Paley, J.M. Wild

Academic Unit of Radiology, University of Sheffield, Royal Hallamshire Hospital, Sheffield S 10 2JF, UK

Received 30 March 2006; revised 16 June 2006
Available online 7 July 2006

Abstract

Slice-multiplexed RF pulses have recently been introduced for simultaneous multi-slice imaging. Their novel aspect is that each slice is given a different linear phase profile, and hence a different slice-rephasing requirement, by the pulse. During readout, extra slice gradients are applied such that when one slice is rephased, the others are dephased to prevent aliasing. In this paper, an improved method of designing slice-multiplexed RF pulses is presented: component pulses which are optimized with simulated annealing for a specific rephasing are combined using Shinnar–Le Roux methods. In this way, non-linearities at higher flip angles are taken into account and more slices can be excited. Bloch simulations show the phase and amplitude profile of component pulses are faithfully preserved in the multiplexed pulse. Three- and four-slice multiplex pulses are demonstrated in gradient- and spin-echo in-vivo imaging.

Keywords: Simultaneous multi-slice imaging; Multiplexed RF pulse; Pulse design; Simulated annealing; Shinnar–Le Roux

1. Introduction

In truly simultaneous multi-slice imaging, a single RF pulse excites multiple slices simultaneously, which then need to be unaliased into separate slices during reconstruction. Many methods can be found in the literature. For example, in the Hadamard phase cycling method, the slices are binary encoded by the RF pulse [1]. Then, for N slices, N extra views are acquired and combined to give the separated slices. In another method, POMP [2], simultaneously excited slices are given a view dependent phase modulation, resulting in slices being shifted to non-overlapping locations in the phase encoding direction. As with Hadamard encoding, for N slices of equivalent size, N extra views are needed. The extra views required in these methods result in increased scanning time. To avoid this, slices may be separated in the frequency encoding direction instead, by shifting the Larmor frequency of each slice by more than the imaging bandwidth. This may be accomplished by either switching on the slice select gradient during readout [3,4], or introducing a stepped field with a B_0 insert coil [5–7]. However, these can lead to distortions if the slice separation is too small [8]. If available, a multicoil receiver system may also be used to unalias the slices, using parallel imaging methods [9,10].

An alternative approach is to rapidly excite multiple slices with closely spaced sequential pulses, followed by a single readout interval with shared phase encoding, as in methods such as MUSIC [11], SER [12], and SD-FLASH [13]. Compared with the methods above, the excitation of slices in these methods will not be truly simultaneous, as the pulses are separated by small dephasing gradient lobes.

Recently, we introduced the slice-multiplexed pulse for simultaneous multi-slice imaging [14]. The single pulse excites multiple slices simultaneously, but such that each slice is given a different linear phase profile. During readout, slices are unaliased by using extra slice-select gradient lobes, which rephase and dephase individual slices one at a time. Thus, the multiplex pulse can be viewed as a fusion of several sequential pulses into the one pulse. In the process,

* Corresponding author.
E-mail address: k.j.lee@sheffield.ac.uk (K.J. Lee).

1090-7807/$ - see front matter © 2006 Elsevier Inc. All rights reserved.
doi:10.1016/j.jmr.2006.06.019

it also removes the need for dephasing gradient lobes in between pulses. Consequently, our method has improved simultaneity compared with sequential slice excitation, but without needing extra views or hardware of truly simultaneous slice methods. The method has recently been used to perform parallel imaging with hyperpolarized ^{3}He [15].

To date, only a two-slice multiplex pulse has been used, constructed by vector summation of an asymmetrically truncated sinc-pulse with its modulated time-reversed equivalent [14,15]. Although vector summation has been used successfully with large flip angles by others [16], it assumes a linear approximation for the Bloch equations, and in theory is not ideal for higher flip angles, or for the higher RF amplitudes expected as more component pulses are added for more slices. Another disadvantage of the simple design is that the range of dephasing was limited to -0.75 to -0.35 of the slice select lobe. Initial experiments showed that to reduce crosstalk, there needs to be approximately a difference of $\geqslant 0.35$ of a slice select lobe between slices. Therefore, a method of incorporating either pure phase pulses, or delayed-focus pulses, which have a positive refocusing lobe, would extend the dephasing range and enable more pulses to be combined. It follows that a necessary step for the development of multiplex pulse imaging is a method of constructing multiplex pulses with three or more slices that overcomes these limitations.

2. Methods

2.1. Pulse design

Our approach for the design of slice-multiplexed pulses combines simulated annealing with the Shinnar–Le Roux (SLR) formalism. Simulated annealing has been widely used to design RF pulses with either zero or positive rephasing [17–20]. The method can thus be used to tune the component pulses with the required linear phase profile. In contrast, although the SLR algorithm can be used to design pulses with a linear phase profile [21–25], this profile cannot be controlled precisely [26,27]. However, it can be used to combine component pulses in a way which takes into account non-linearities of the Bloch equations.

We illustrate the method with a detailed description of the design of a 3-slice multiplex pulse. First, we require 3 component pulses with different rephasing requirements. For the first component pulse, P1, we used a DBURP1 pulse [28], with a rephasing of +0.15 of the slice select lobe. The other pulses were in-house pulses constructed by simulated annealing, following almost exactly the method of Geen and Freeman [17]. The pulses were amplitude-modulated, and characterized by a finite Fourier series:

$$\frac{\gamma B_1(t)}{2\pi} = \frac{1}{T}\left\{a_0 + \sum_{n=1}^{m}[a_n \cos(n\omega t) + b_n \sin(n\omega t)]\right\} \qquad (1)$$

where $\omega = 2\pi/T$ and T is the pulse duration. The maximum number of attempted uphill climbs was set to $N_a = 500(2m+1)$, where m is the number of Fourier coefficients in Eq. (1), chosen to be 6 in this work. The maximum number of successful uphill climbs was set to $N_s = 0.1N_a$. Either of these limits must be attained before the temperature was reduced, following an annealing schedule of $T_i/T_{i-1} = 0.99975$. To obtain a dephasing separation of 0.5 of a slice select lobe between each of the

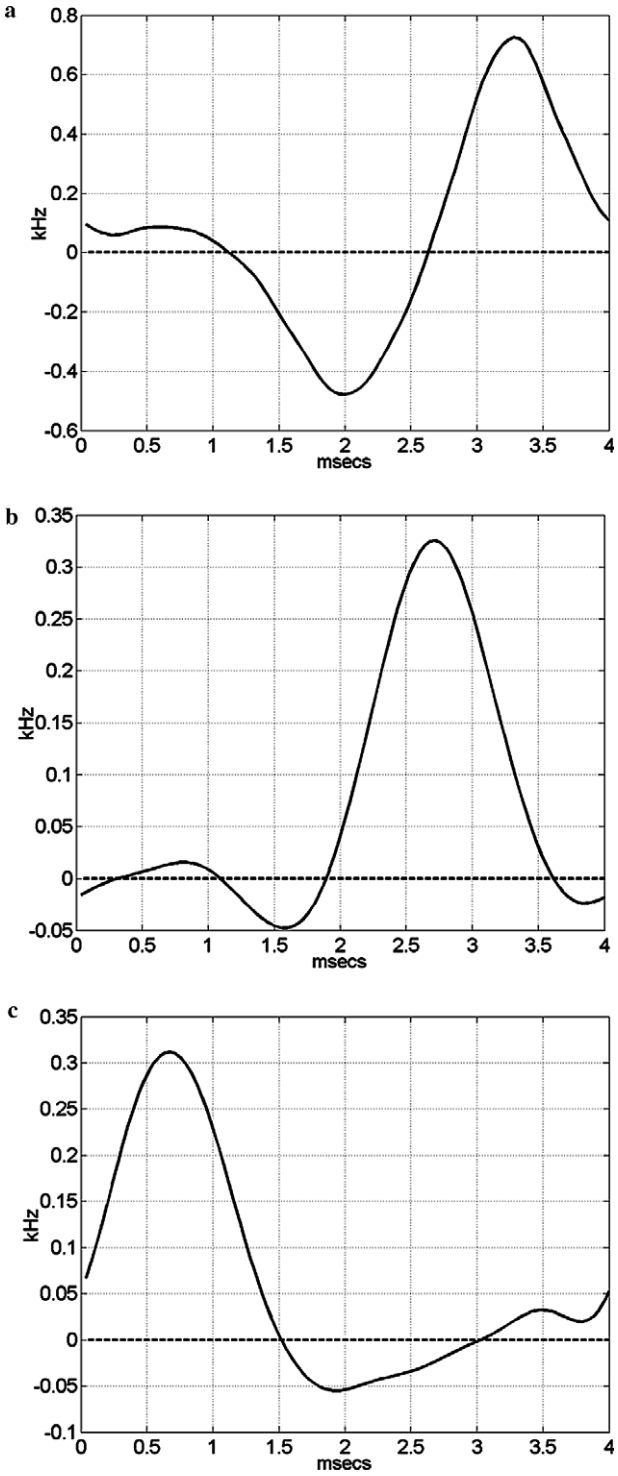

Fig. 1. Component pulses for 3-slice multiplex pulse. Real (solid), imaginary (dashed). (a) P1 (b) P2 (c) P3.

components, component pulse P2 was designed with a rephasing of −0.35, and pulse P3 with a rephasing of −0.85. The pulses are shown in Fig. 1 and their Fourier coefficients are shown in Table 1. All component pulses were constructed from Fourier coefficients with 100 points, dwell times of 40 μs, giving a total duration of 4 ms, and were scaled to have a slice width of 1 kHz. The next step is to combine pulses P1, P2, and P3 into a single, composite multiband pulse using the SLR algorithm.

In the SLR algorithm, an RF pulse is approximated as a series of hard pulses, each responsible for a small rotation of the magnetization vector. Through spinor notation, the total rotation caused by the pulse can be described by two z-transform polynomials, called the SLR A and B polynomials [25]. Calculation of the polynomials from the pulse is known as the forward SLR transform. The reverse procedure is the inverse SLR transform, which generates the RF pulse from given A and B polynomials, usually constructed according to the desired slice profile through the Parks–McClellan algorithm.

We now describe briefly the method by Cunningham and Wood for combining RF pulses to excite multibands [29]. They recognised that while the relation between RF pulse and excitation profiles, described by the Bloch equations, is non-linear at large flip angles, the relationship between component B polynomials and their excitation profiles is approximately linear. Therefore, component B polynomial can be modulated and added together to form a composite B polynomial. This key observation is the essence of the Cunningham and Wood method of creating multiband pulses. The composite minimum power A polynomial, $A(z)$, is then derived from the composite B polynomial, $B(z)$, through the equations [25]:

$$|A(z)| = \sqrt{1 - B(z)B^*(z)} \qquad (2)$$
$$\arg\{A(z)\} = H\{\log|A(z)|\}$$

where H is the Hilbert transform operator. The composite A and B polynomials are then inverse SLR transformed to give the desired composite multiband RF pulse. In their paper, Cunningham and Wood also included a correction for the position-dependent slice-walk phase error. We will not be including this correction, as slice-walk is not a problem if only magnitude images are used, as in this work. However, slice-walk should be corrected if multiplex pulses were to be used for phase-sensitive studies, e.g., Hadamard encoding [1].

Note that one characteristic of the minimum power A polynomial is that its roots are all inside the unit circle, and thus a straightforward application of the Cunningham and Wood method will not work if any of the component A polynomial is not originally minimum power, as this property is lost when generating the A polynomial for the composite B polynomial. Consider Figs. 2a–c which show the roots of the A polynomial for the component pulses, obtained by forward SLR transforming pulses P1, P2, and P3, respectively. We note that two of the roots for the DBURP1 pulse P1 are outside the unit circle. Therefore, a delayed-focus pulse like the DBURP1 pulse will lose its positive rephasing property if combined into a single multiband pulse with the Cunningham and Wood method. Fig. 2d shows the combined B polynomial, obtained by adding the component B polynomials (after modulating the polynomial corresponding to P1 to shift its response by −6.25 kHz, the polynomial corresponding to P3 by +6.25 kHz, and leaving P2's polynomial unmodulated). The roots of the minimum power A polynomial from the combined B polynomial is shown in Fig. 2e. Note that the two P1 roots which were outside the unit circle are now inside. The modification we make to the Cunningham and Wood method is simply to reflect these roots back outside the unit circle as shown in Fig. 2f. The justification for this lies in the observation by Pickup and Ding that inverting the roots of the A or B polynomial does not affect their overall magnitude [26]. Therefore, if the magnitudes of the combined A and B polynomials within the selected band of P1 remain the same as in the component pulse, the roots of the A polynomial can only be in either their original or their reflected positions. Therefore, by reflecting the roots of P1 back to their original positions, we can restore the phase profile. After the reflections, the resulting A polynomial, taken with the combined B polynomial of Fig. 2d, are inverse SLR transformed to give the final 3-slice multiplexed pulse shown in Fig. 2g.

The public-domain MATPULSE software (version 2.4) was used to perform a Bloch simulation of the pulse [30]. The simulation of the component pulses are shown in

Table 1
Fourier coefficients for component pulses

	P1	P2	P3
Rephasing	+0.15	−0.35	−0.85
a_0	0.25	0.2808	0.2576
a_1	1.25	−0.2324	0.3800
a_2	−0.98	−0.2025	−0.1921
a_3	−0.15	0.0842	−0.1275
a_4	−0.03	0.0035	−0.0329
a_5	0.04	0.0017	−0.0124
a_6	0.00	0.0021	−0.0041
a_7	0.00	—	—
a_8	−0.01	—	—
a_9	0.00	—	—
a_{10}	0.00	—	—
a_{11}	0.00	—	—
a_{12}	0.01	—	—
b_1	−0.95	−0.4841	0.4155
b_2	−0.34	0.3377	0.2475
b_3	0.13	−0.0143	0.0043
b_4	0.11	−0.0046	0.0034
b_5	−0.01	0.0058	0.0069
b_6	−0.01	0.0031	0.0083
b_7	−0.01	—	—
b_8	0.00	—	—
b_9	0.00	—	—
b_{10}	0.01	—	—
b_{11}	0.01	—	—
b_{12}	0.00	—	—

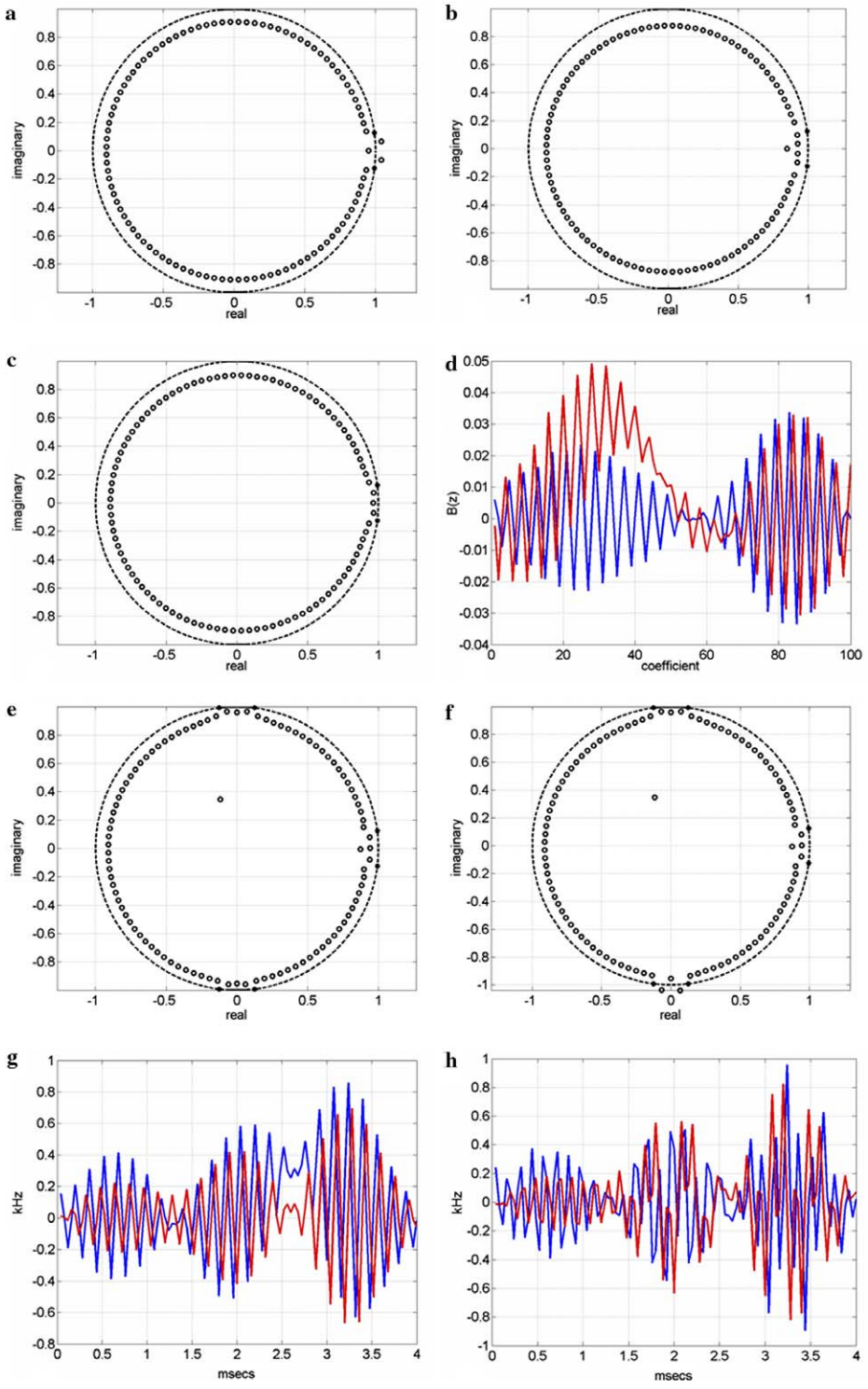

Fig. 2. (a) Roots of A polynomial for P1; the passband is indicated by asterisks on the unit circle (b) roots of A polynomial for P2 (c) roots of A polynomial for P3. (d) Coefficients of combined B polynomial, after the component B polynomials have been modulated and summed. Real part (blue) and imaginary part (red). (e) Roots of composite minimum power A polynomial (f) roots of A polynomial after roots of P1 are flipped back outside the unit circle (g) 3-slice multiplex pulse. (h) 4-slice multiplex pulse.

Figs. 3a–c. Figs. 3d–f show the simulation of the multiplex pulse with the corresponding rephasing. Figs. 3g–i show the result of subtracting the profiles of Figs. 3a–c from Figs. 3d–f, indicating that the amplitude and phase response of the components are preserved faithfully in the multiplex pulse.

A 4-slice multiplexed pulse was also similarly created using component pulses with rephasing +0.15, −0.19,

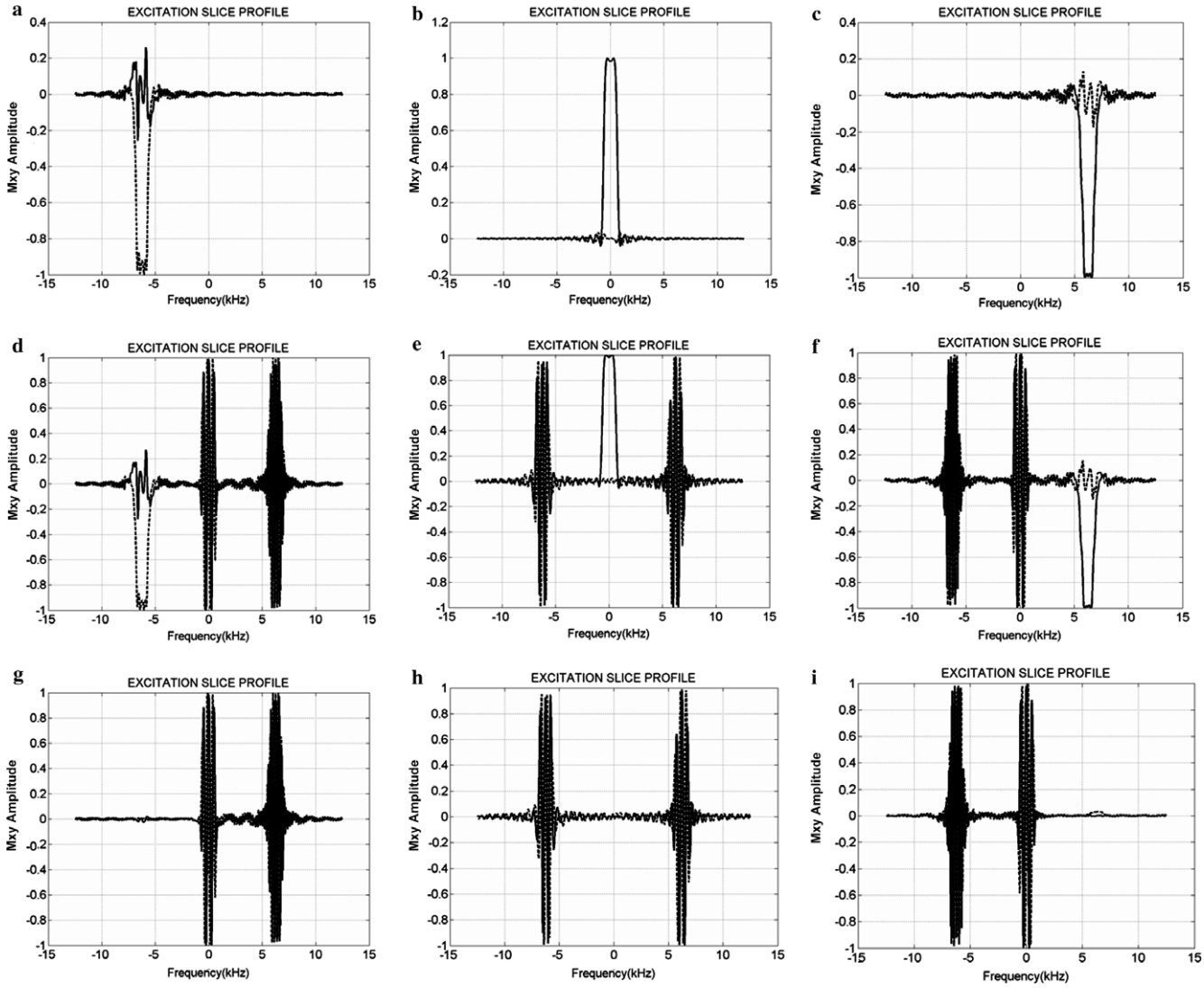

Fig. 3. Bloch simulations with MATPULSE (a) P1: rephasing +0.15 (b) P2: rephasing −0.35 (c) P3: rephasing −0.85 (d) multiplex pulse: rephasing +0.15 (e) multiplex pulse: rephasing −0.35 (f) multiplex pulse: rephasing −0.85 (g) d − a (h) e − b (i) f − c.

−0.5, and −0.85 of the slice-select lobe. They were modulated to excite slices at frequencies of ±2.5 and ±5 kHz. The pulse is shown in Fig. 2h.

2.2. Gradient-echo

To reduce aliasing, the 3- and 4-slice pulses were first interpolated to 400 time points, with a dwell time of 10 μs. The pulses were then implemented in a gradient-echo sequence, with one echo per slice. A schematic of the 3-slice sequence is shown in Fig. 4. Imaging was performed on an 1.5 T scanner (Eclipse; Philips Medical Systems, Cleveland, OH, USA) with a maximum gradient strength of 27 mT/m and a rise time to maximum of 350 μs. Axial brain images were acquired from normal volunteers, with flip angle = 90°, TR = 200 ms, matrix size = 256 × 256, slice thickness = 2 mm, number of averages (NSA) = 1.

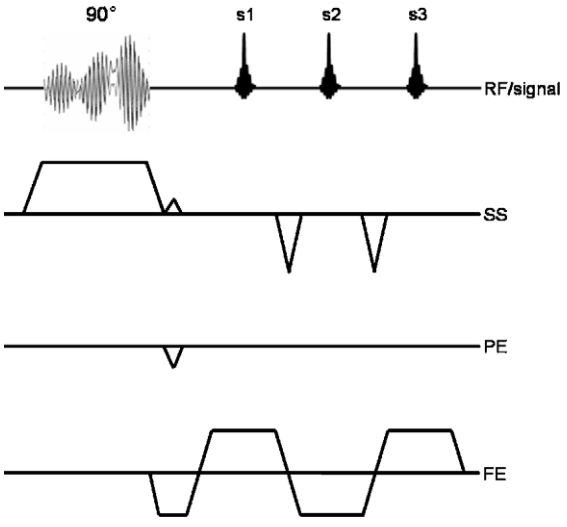

Fig. 4. Schematic gradient-echo pulse sequence for 3-slice multiplex pulse.

The TEs from the center of the RF pulse were 5.3, 7.6, and 9.9 ms for the first three echoes, and 12.2 ms for the fourth.

2.3. Spin-echo

The 3-slice pulse was used as the excitation pulse in a spin-echo sequence on the same scanner. The sequence is similar to the GRASE sequence [31], with the difference that in our sequence, during each spin-echo, each gradient echo collects the same *k*-space line from a different slice, rather than different *k*-space lines from the same slice. A schematic of the sequence is shown in Fig. 5. Only the first two spin-echoes are shown; in fact, four spin-echoes were collected per view. The second gradient-echoes coincided with the spin-echoes which were refocused at TE = 45, 121, 197, and 273 ms. The first and third gradient-echoes were acquired at 3.1 ms either side of the second gradient-echo. The design for crusher gradients around the non-slice selective refocusing pulse was taken from Ref. [32]. Axial brain images were acquired from a normal volunteer, with flip angle = 90°, TR = 2500 ms, matrix size = 256 × 128, slice thickness = 4 mm, and NSA = 3.

3. Results

3.1. Gradient echo

Figs. 6a–c show images obtained from the 3-slice gradient-echo sequence. Images from the 4-slice gradient-echo sequence are shown in Figs. 7a–d. The slices from both sequences show different SNR. This arises not just because of different echo times, but because the slices were designed with different ripple amplitudes and is a disadvantage of our present method. The first slice in Figs. 6 and 7, corresponding to the DBURP1

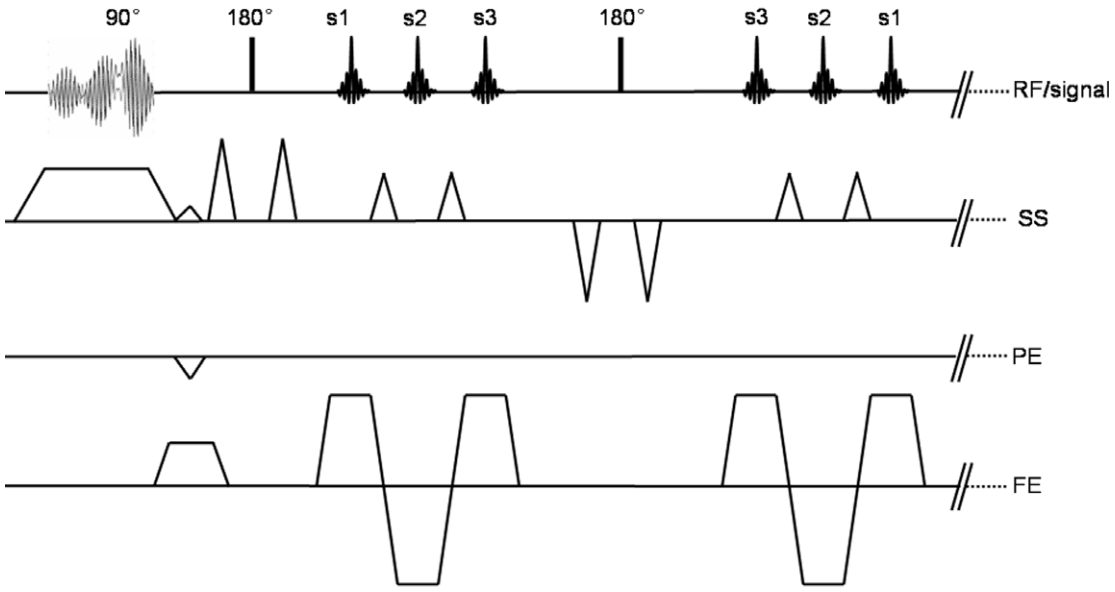

Fig. 5. Schematic spin-echo sequence for 3-slice multiplex pulse. Note that only the first two (out of four actually implemented) spin-echoes are shown.

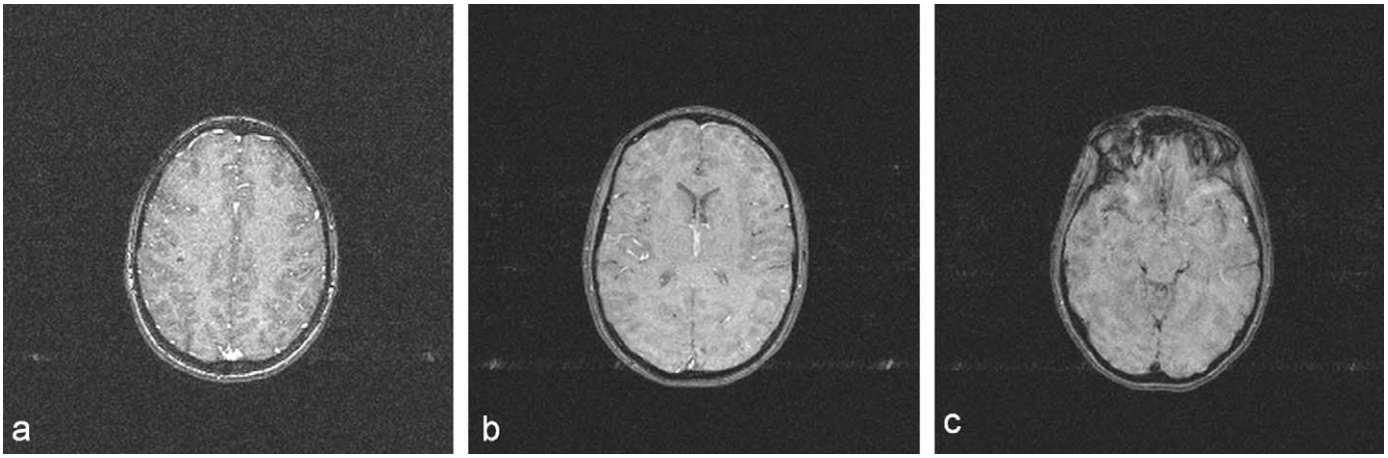

Fig. 6. Gradient-echo images from 3-slice multiplex pulse. (a) Echo 1 (b) echo 2 (c) echo 3.

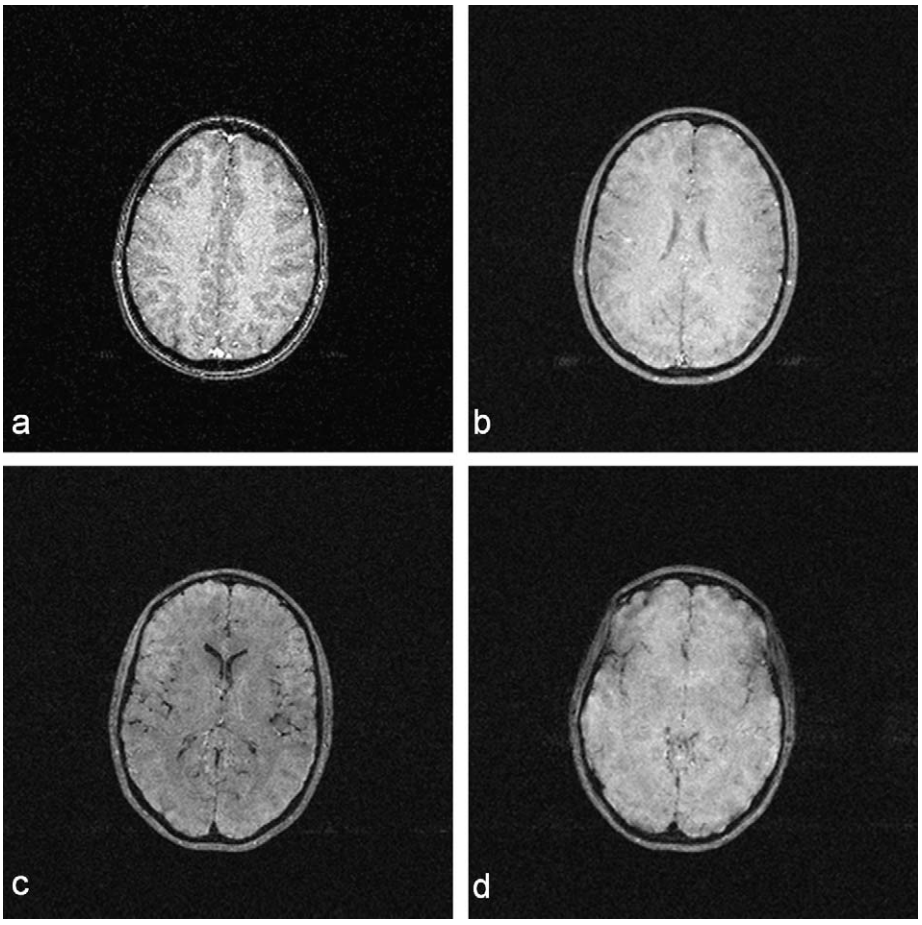

Fig. 7. Gradient-echo images from 4-slice multiplex pulse. (a) Echo 1 (b) echo 2 (c) echo 3 (d) echo 4.

component, has the lowest SNR in spite of having the shortest TE, reflecting its relatively large in-slice ripple.

3.2. Spin echo

Fig. 8 shows the images obtained from the spin-echo sequence. The images show increasing T2 weighting, as expected. Although the slice thickness is 4 mm, there are no visible crosstalk artifacts due to susceptibility gradients, indicating effective spin-echo refocusing. Also, the differences in SNR between slices are not nearly as marked as those in the gradient echo images.

4. Discussion

The results show that by combining simulated annealing with SLR methods, multiplex pulses have been obtained that can be used at higher flip angles, with more slices and with greater dephasing between slices than previously demonstrated [14].

In our experience, we find that for our 4 ms, 1 kHz width pulse, only pulses with a rephasing between -0.85 and $+0.2$ gave acceptable SNR. Furthermore, in practice, the minimum dephasing required to prevent significant crosstalk between slices was approximately 0.35 of a slice-select lobe, corresponding to a phase twist of 8.8 radians across the slice. This would put a maximum limit of about 4 slices in a 4 ms, 1 kHz width multiplex pulse.

It is not possible to control the magnitude of the linear phase ramp with the SLR algorithm. Therefore, we used simulated annealing to design component pulses because this method can, with sufficiently slow annealing, find the global minimum pulse for given a cost function. Unfortunately, we lose direct control over other parameters such as the amplitude ripple in the slice profile. As a result, the slices have different SNR, because the in-slice ripple reflects the amount of dephasing within the slice. In a perfect system, if there were no other sources of dephasing, the SNR would be the same in both gradient and spin echoes. However, because of imperfect gradient refocusing, or the presence of field inhomogeneities, the dephasing has a bigger impact on the gradient echoes. This is consistent with further experiments (data not shown) which show that SNR in the slices with large ripples approach the SNR of slices with small ripples as the slice thickness is reduced. It would also explain why spin-echoes were not affected to the same extent, with very similar SNR between slices (see Fig. 8). In future, we will examine ways to overcome variable SNR, for

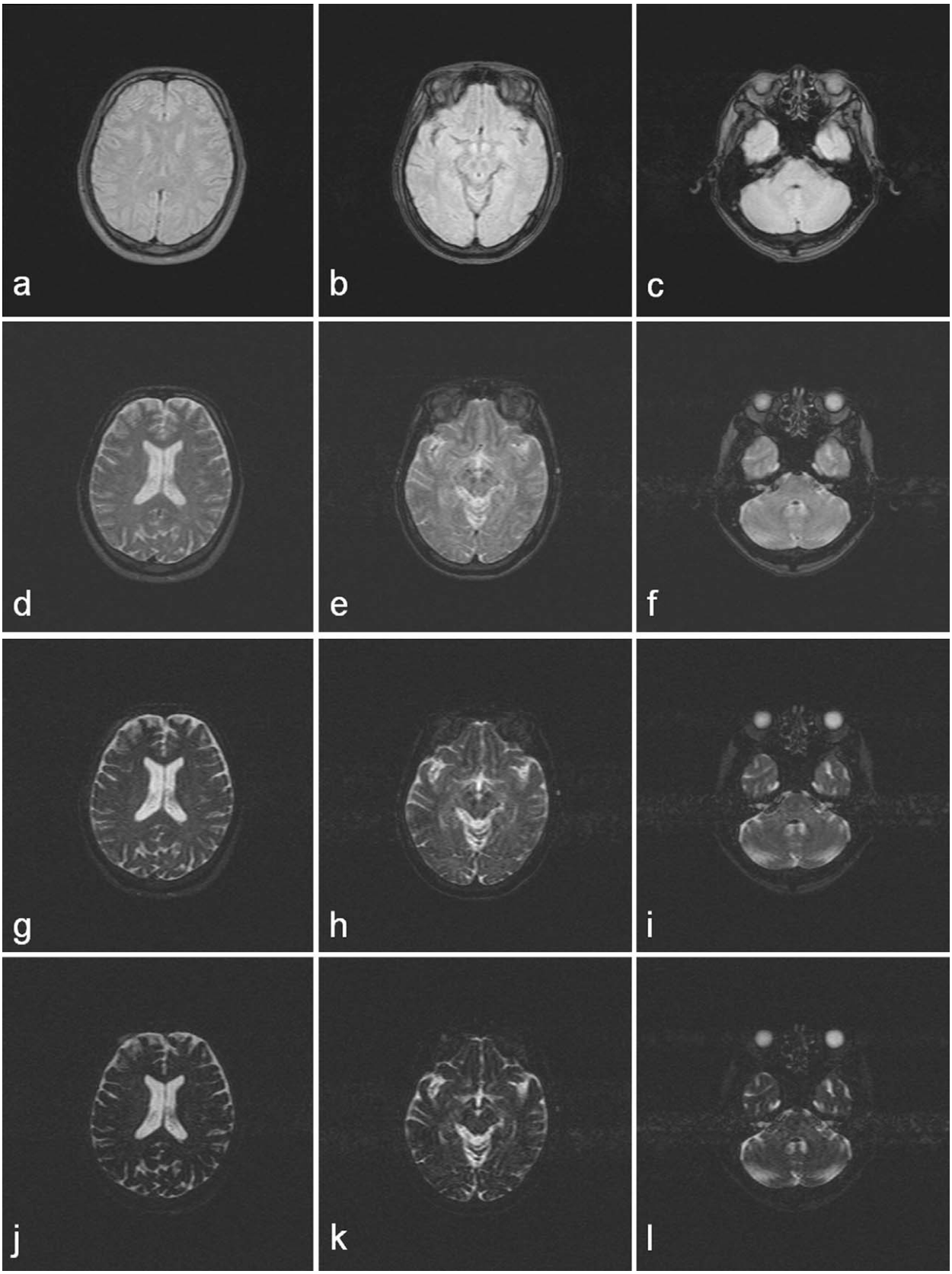

Fig. 8. Spin-echo images from 3-slice multiplex pulse. The images have been re-arranged so that rows correspond to echo number, and columns correspond to slice number.

instance, by modifying the cost function of Geen and Freeman to include ripple amplitudes, or using other pulse design methods such as the inverse scattering transform (IST) which give direct control over slice amplitude and phase [33–36].

Armed with this method of constructing a multiplexed pulse which faithfully retains the phase profile of the component pulses, we will be examining other applications for it. One possible application is faster multi-slice imaging. For example, in a gradient-echo sequence, to image four slices, the multiplexed sequence will be faster than a conventional sequence if its total time for one view of (1 multiplex pulse + 1 phase encode + 4 readouts) is less than (4 conventional pulses + 4 phase encodes + 4 readouts). Another advantage of the multiplex pulse is, as with the GRASE sequence, the utilisation of time in between refocusing pulses in multiple spin-echo imaging. In the GRASE sequence, this time is used to acquire more *k*-space lines for one slice. The multiplex pulse allows this time to be used for acquiring more slices. For example, the sequences presented above could be modified to allow multi-slice T2 and T2* relaxometry, Dixon fat-water imaging, or faster dual proton-density/T2 weighted spin-echo sequence, currently the workhorse of brain imaging.

5. Conclusion

A new method has been described for the design of multiband slice-multiplexed pulses. Component pulses with the required linear phase profile are designed using simulated annealing. These pulses are forward SLR transformed to obtain their A and B polynomials. Any A polynomial roots that are outside the unit circle are noted. The component B polynomial is then modulated and summed, and the combined B polynomial used to generate a combined A polynomial, as described by Cunningham and Wood. However, because this results in a combined minimum power A polynomial, any roots that were originally outside the unit circle are reflected back outside before the inverse SLR transform to generate the multiplex pulse. The resulting pulses have been shown to retain the amplitude and phase responses of their components. Future work will be directed at improving the variability of SNR between slices and in applications of the multiplex pulse for faster multi-slice imaging.

Acknowledgments

K.J. Lee was supported by an EPSRC First Grant Scheme award (EP/C537491/1). J.M. Wild was supported by EPSRC Grant GR/S81834/01(P).

References

[1] S.P. Souza, J. Szumowski, C.L. Dumoulin, D.P. Plewes, G. Glover, SIMA: simultaneous multislice acquisition of MR images by Hadamard-encoded excitation, J. Comput. Assist. Tomogr. 12 (1988) 1026–1030.
[2] G.H. Glover, Phase-offset multiplanar (POMP) volume imaging: a new technique, J. Magn. Reson. Imaging 1 (1991) 457–461.
[3] M.N. Paley, K.J. Lee, J.M. Wild, P.D. Griffiths, E.H. Whitby, Simultaneous parallel inclined readout image technique, Magn. Reson. Imaging 24 (2006) 557–562.
[4] J.B. Weaver, Simultaneous multislice acquisition of MR images, Magn. Reson. Med. 8 (1988) 275–284.
[5] K.J. Lee, M.N. Paley, I.D. Wilkinson, P.D. Griffiths, Magnetic resonance imaging with stepped B-0 fields, Magn. Reson. Imaging 21 (2003) 625–629.
[6] M.N. Paley, K.J. Lee, J.M. Wild, S. Fichele, E.H. Whitby, I.D. Wilkinson, E.J. van Beek, P.D. Griffiths, B1AC-MAMBA: B1 array combined with multiple-acquisition micro B0 array parallel magnetic resonance imaging, Magn. Reson. Med. 49 (2003) 1196–1200.
[7] M.N.J. Paley, K.J. Lee, J.M. Wild, E.H. Whitby, P.D. Griffiths, Interleaved pulsed MAMBA: a new parallel slice imaging method, Magn. Reson. Med. 48 (2002) 1043–1050.
[8] K.J. Lee, M.N.J. Paley, D.C. Barber, I.D. Wilkinson, P.D. Griffiths, Target field design for MAMBA step fields, Concepts Magn. Reson. Part B-Magn. Reson. Eng. 20B (2004) 1–8.
[9] F.A. Breuer, M. Blaimer, R.M. Heidemann, M.F. Mueller, M.A. Griswold, P.M. Jakob, Controlled aliasing in parallel imaging results in higher acceleration (CAIPIRINHA) for multi-slice imaging, Magn. Reson. Med. 53 (2005) 684–691.
[10] D.J. Larkman, J.V. Hajnal, A.H. Herlihy, G.A. Coutts, I.R. Young, G. Ehnholm, Use of multicoil arrays for separation of signal from multiple slices simultaneously excited, J. Magn. Reson. Imaging 13 (2001) 313–317.
[11] T. Loenneker, F. Hennel, J. Hennig, Multislice interleaved excitation cycles (MUSIC): an efficient gradient-echo technique for functional MRI, Magn. Reson. Med. 35 (1996) 870–874.
[12] D.A. Feinberg, T.G. Reese, V.J. Wedeen, Simultaneous echo refocusing in EPI, Magn. Reson. Med. 48 (2002) 1–5.
[13] W.H. Perman, M.H. Gado, K.B. Larson, J.S. Perlmutter, Simultaneous MR acquisition of arterial and brain signal-time curves, Magn. Reson. Med. 28 (1992) 74–83.
[14] K.J. Lee, J.M. Wild, P.D. Griffiths, M.N. Paley, Simultaneous multislice imaging with slice-multiplexed RF pulses, Magn. Reson. Med. 54 (2005) 755–760.
[15] K. Teh, K.J. Lee, M.N.J. Paley, J.M. Wild, Parallel imaging of hyperpolarized helium-3 with simultaneous slice excitation, Magn. Reson. Med. 55 (2006) 258–262.
[16] E. Kupce, R. Freeman, Techniques for multisite excitation, J. Magn. Reson. A 105 (1993) 234–238.
[17] H. Geen, R. Freeman, Band-selective radiofrequency pulses, J. Magn. Reson. 93 (1991) 93–141.
[18] H. Geen, S. Wimperis, R. Freeman, Band-selective pulses without phase-distortion—a simulated annealing approach, J. Magn. Reson. 85 (1989) 620–627.
[19] T.P.L. Roberts, T.A. Carpenter, L.D. Hall, Design and application of prefocused pulses by simulated annealing, J. Magn. Reson. 89 (1990) 595–604.
[20] J. Shen, Delayed-focus pulses optimized using simulated annealing, J. Magn. Reson. 149 (2001) 234–238.
[21] P. Le Roux, Exact synthesis of radiofrequency waveforms, Proceedings of 7th Meeting of the Society for Magnetic Resonance in Medicine (1988) 1049.
[22] M. Shinnar, S. Eleff, H. Subramanian, J.S. Leigh, The synthesis of pulse sequences yielding arbitrary magnetization vectors, Magn. Reson. Med. 12 (1989) 74–80.
[23] M. Shinnar, L. Bolinger, J.S. Leigh, The use of finite impulse response filters in pulse design, Magn. Reson. Med. 12 (1989) 81–87.
[24] M. Shinnar, J.S. Leigh, The application of spinors to pulse synthesis and analysis, Magn. Reson. Med. 12 (1989) 93–98.

[25] J. Pauly, P. Leroux, D. Nishimura, A. Macovski, Parameter relations for the Shinnar–Le Roux selective excitation pulse design algorithm, IEEE Trans. Med. Imaging 10 (1991) 53–65.
[26] S. Pickup, X.N. Ding, Pulses with fixed magnitude and variable phase response profiles, Magn. Reson. Med. 33 (1995) 648–655.
[27] S. Pickup, M. Popescu, Efficient design of pulses with trapezoidal magnitude and linear phase response profiles, Magn. Reson. Med. 38 (1997) 137–145.
[28] X.L. Wu, P. Xu, R. Freeman, Delayed-focus pulses for magnetic-resonance-imaging—an evolutionary approach, Magn. Reson. Med. 20 (1991) 165–170.
[29] C.H. Cunningham, M.L. Wood, Method for improved multiband excitation profiles using the Shinnar–Le Roux transform, Magn. Reson. Med. 42 (1999) 577–584.
[30] G.B. Matson, An integrated program for amplitude-modulated RF pulse generation and re-mapping with shaped gradients, Magn. Reson. Imaging 12 (1994) 1205–1225.
[31] K. Oshio, D.A. Feinberg, GRASE (Gradient- and spin-echo) imaging: a novel fast MRI technique, Magn. Reson. Med. 20 (1991) 344–349.
[32] C.S. Poon, R.M. Henkelman, Practical T2 quantitation for clinical applications, J. Magn. Reson. Imaging 2 (1992) 541–553.
[33] J. Magland, C.L. Epstein, Practical pulse synthesis via the discrete inverse scattering transform, J. Magn. Reson. 172 (2005) 63–78.
[34] D.E. Rourke, P.G. Morris, The inverse scattering transform and its use in the exact inversion of the Bloch equation for noninteracting spins, J. Magn. Reson. 99 (1992) 118–138.
[35] M.H. Buonocore, RF pulse design using the inverse scattering transform, Magn. Reson. Med. 29 (1993) 470–477.
[36] P. Kozlowski, D.E. Rourke, B.G. Winsborrow, J.K. Saunders, Highly prefocused selective pulses—a tool for in vivo 31P spectroscopic imaging, J. Magn. Reson. B 104 (1994) 280–283.